Coalescence aspects of cobalt nanoparticles during in situ high-temperature annealing

Palasantzas, G.; Vystavel, T.; Koch, S. A.; De Hosson, J. Th. M.

Published in:
Journal of Applied Physics

DOI:
10.1063/1.2163983

Publication date:
2006

Coalescence aspects of cobalt nanoparticles during *in situ* high-temperature annealing

G. Palasantzas,[a] T. Vystavel, S. A. Koch, and J. Th. M. De Hosson
Department of Applied Physics, Materials Science Centre and the Netherlands Institute for Metals Research, University of Groningen, 9747 AG Groningen, The Netherlands

(Received 3 May 2005; accepted 12 December 2005; published online 24 January 2006)

In this work we investigate the coalescence aspects of Co nanoparticles. It was observed that nanoparticles in contact with the substrate are relatively immobile, whereas those on top of other Co particles can rearrange themselves during high-temperature annealing and further coalesce. Indeed, similar size particles prior to coalescence come at close proximity forming an arc-shaped area, which leads to finite-size necking and thereafter to coalescence towards a single partially spherical particle. This is in contrast to the theoretical predictions where necking occurs following an initial pathway of a point contact. Moreover, it was shown that after necking a transient period of relatively fast coalescence occurs followed by a slower coalescence rate at constant speed towards a single particle with partial spherical shape. In addition, the coalescence is faster with decreasing particle size, where in the case of unequal size the smallest particle is mainly absorbed by an adjacent large one in an Ostwald ripening process. © *2006 American Institute of Physics*.
[DOI: 10.1063/1.2163983]

I. INTRODUCTION

Various studies have revealed that nanoparticles of several elements often show anomalies in the phase transformation and the phase stability, resulting in metastable and unique crystal phases that are quite different from the bulk specimens.[1–8] The studies of magnetic nanoparticles are important since future magnetic media will require higher bit densities. For Co (Refs. 1–3, 7, and 9) the particles (below a certain size) crystallize in the high-temperature fcc phase that is only stable above 420 °C in bulk form.[10] For Co nanoparticles with average diameter D less than 50 nm (synthesized by sputtering Co in a relatively high inert-gas pressure) it has been found that there is a close relationship between the particle size and the crystal phase.[11] It was determined to be pure fcc (β phase) for $D<20$ nm, a mixture of hcp (α phase) and fcc phases for $D\approx 30$ nm, and an α phase with inclusion of a very small amount of β phase for $D>40$ nm.[11]

Structural characterizations by transmission electron microscopy[11] (TEM) have revealed that the β-phase particles are multiply twinned icosahedrons and the α-phase particles are perfect single crystals with an external shape of a Wulff polyhedron. Theoretical calculations have explained the size dependence of the crystal phase of the Co fine particles, and have revealed that the stabilization of β phase is an intrinsic effect caused by the small dimensionality of the nanoparticles (due to lower surface energy). The allotropic $\beta\rightarrow\alpha$ transformation is strongly inhibited down to 28 K, and therefore the β phase is energetically stable.[12] In addition, magnetic measurements have revealed a correlation between coercivity and particle size where an increase in particle size enhances the coercivity considerably due to the hcp phase.[12]

So far Co nanoparticle coalescence has not be studied in great detail despite the fact that it is important due to the dependence of the crystal structure on particle size, which further influence the magnetic properties. Recently, particle-particle coalescence process of monodispersed Co particles with mean diameter $d=8.5$ and 13 nm was investigated by *in situ* electrical conductivity measurements, and TEM.[12] The electrical conductivity measurements and TEM observations indicated that for $T<100$ °C the Co particles in the assemblies maintained their original structure as deposited at room temperature. On the other hand in this work we will estimate particle coalescence times and the corresponding diffusion coefficients at elevated temperatures, and we will compare our findings with theoretical predictions.

II. EXPERIMENTAL PROCEDURE

Particle deposition was performed using the NC200U source manufactured by Oxford Applied Research.[13] It is based on the gas aggregation technique,[13] using magnetron sputtering to create atomic vapor. This method provides a relatively monodisperse particle size distribution (statistical variation in particle diameter is approximately 10%). Sputtered atoms combine in a flow of Ar gas (pressure ~0.3 mbar) to form nanoparticles. The chamber base pressure was about 10^{-8} mbar. The magnetron power was 70–90 W. The deposition yielded low-energy-deposited particles, which preserve their integrity upon impact onto the substrate. Particles were deposited on carbon-coated (10 nm thick) Cu grids and on Si_3N_4 support films of thickness of 20 nm for TEM analysis in a JEOL 2010F transmission electron microscope. The latter is equipped with a double tilt heating specimen holder allowing to heat the samples up to 850 °C. The samples were briefly exposed to air during the transfer to the microscope.

[a]Author to whom correspondence should be addressed; electronic mail: g.palasantzas@rug.nl

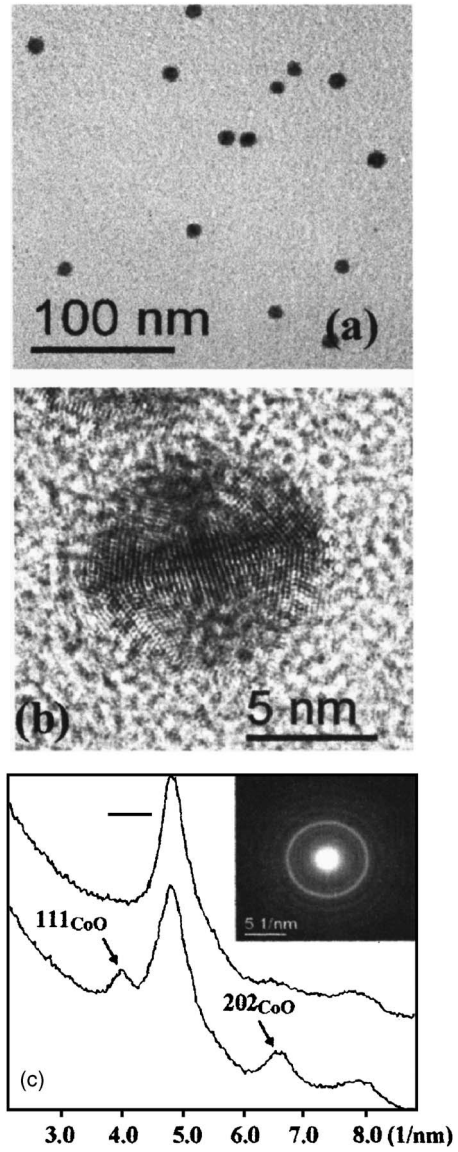

FIG. 1. (a) TEM image of uniformly sized Co nanoparticles deposited on C-coated film. (b) TEM image of an icosahedral Co nanoparticle viewed along the twofold axis. (c) Electron-diffraction pattern obtained on a continuous Co nanoparticle film with arrows indicating peaks arising from CoO.

III. RESULTS AND DISCUSSION

Figure 1(a) shows a TEM image of rather uniform in size randomly deposited Co particles, and a typical isolated Co particle (supported on a carbon-coated grid) of the icosahedral two-dimensional (2D) projected shape. The icosahedron is viewed along its *twofold* symmetry axis, while other particles were observed to be in the *threefold* or *fivefold* orientations. Electron-diffraction measurements [Fig. 1(c)] indicate a predominant fcc crystal phase in these samples, including only a small amount of hcp phase. The fraction of Co bulk phase (hcp) is known to increase with increasing nanoparticle size.[14] In addition, fcc CoO was detected, although the oxide peaks were more pronounced in some samples than in others [Fig. 1(c)], due to different times of exposure to air (the TEM samples were transferred into the electron microscope without a protective capping layer). In ambient air Co nanoparticles form an oxide shell of about 1 nm thick, while smaller particles (2 nm) are completely converted into CoO. The TEM images [Fig. 1(b)] suggest that the oxide thickness is less than 1 nm, contrary to the earlier case of Fe particles where the shell was significantly larger in thickness (2 nm).[15] Coalescence will begin after CoO breaks up at relatively low temperatures ($>200\ ^\circ$C).

In general the crystal structure and habit of nanoparticles depend on temperature and composition. In many cases the particles have a polyhedral form with various degrees of truncation. These shapes occur since they lead to surface energy minimization for particles formed at equilibrium, or because of kinetics where the shape is determined by the rate at which different crystal faces grow. The combination of factors such as temperature, kinetics, impurities, and surface energy effects could lead to unusual nanoparticle size-shape distributions,[14] which influence particle coalescence.

Figure 2 shows various temporal stages of particle coalescence during annealing at 850 °C. An estimate of the coalescence time for particles of similar diameter (e.g., 30 nm) yields a value for τ_c of about 40 s if we assume that the coalescence starts in Fig. 2(b) and being completed in Fig. 2(d). The driving force for coalescence is atomic diffusion. In the case of surface diffusion, atoms diffuse on the particle surface from the regions of high curvature (fewer neighbors and therefore less strongly bound) towards the regions of lower curvature. Long coalescence times have been attributed to the presence of facets and edges on the initial particle surface that persist and rearrange during coalescence. For facets the curvature is zero, and so is the driving force for surface diffusion. Also edge barriers due to edges between facets can slow down diffusion of atoms even further.[15] In addition, with decreasing particle size the coalescence time decreases. This is shown in Fig. 3 where a small particle of radius R of 5 nm coalesces with a much larger one during annealing at 700 °C. The corresponding coalescence time is around 20 s, which is lower than in Fig. 2 despite the significantly lower annealing temperature. The situation in Fig. 3 is a typical case of Ostwald ripening where a smaller particle is absorbed by a larger one.

Macroscopic theories of coalescence via atomic surface diffusion predict a coalescence time,[16]

$$\tau_c = [(k_B T)/(C D_s \gamma)](R/a)^4, \tag{1}$$

with R the nanoparticle radius, γ the surface energy, C a numerical constant (≈ 25), D_s the surface diffusion constant, and $a \approx 0.3$ nm an atomic dimension size. For the particles of Fig. 2 with $R \approx 15$ nm, $T = 1123$ K, $a = 0.3$ nm, and $\gamma = 2.8\ \mathrm{J/m^2}$ (Ref. 17) we obtain $D_s \approx 1.7 \times 10^{-17}\ \mathrm{m^2\ s^{-1}}$ if we use the experimental value $\tau_c \approx 40$ s. If we estimate the distance that an atom travels within the coalescence time $\tau_c \approx 40$ s using the relation $D_{\mathrm{dif}} = \sqrt{D_s \tau_c}$ we obtain $D_{\mathrm{dif}} = 26$ nm which is comparable with the radius of the particle size after coalescence. On the other hand for the coalescence at 700 °C in Fig. 3, Eq. (1) predicts much larger time than the experimental one of 20 s indicating that surface diffusion is not the only operative process and indeed Ostwald ripening also operates. In addition, the TEM analysis showed that particle coalescence occurs more easily for particles supported onto other Co particles. Indeed, particles in contact

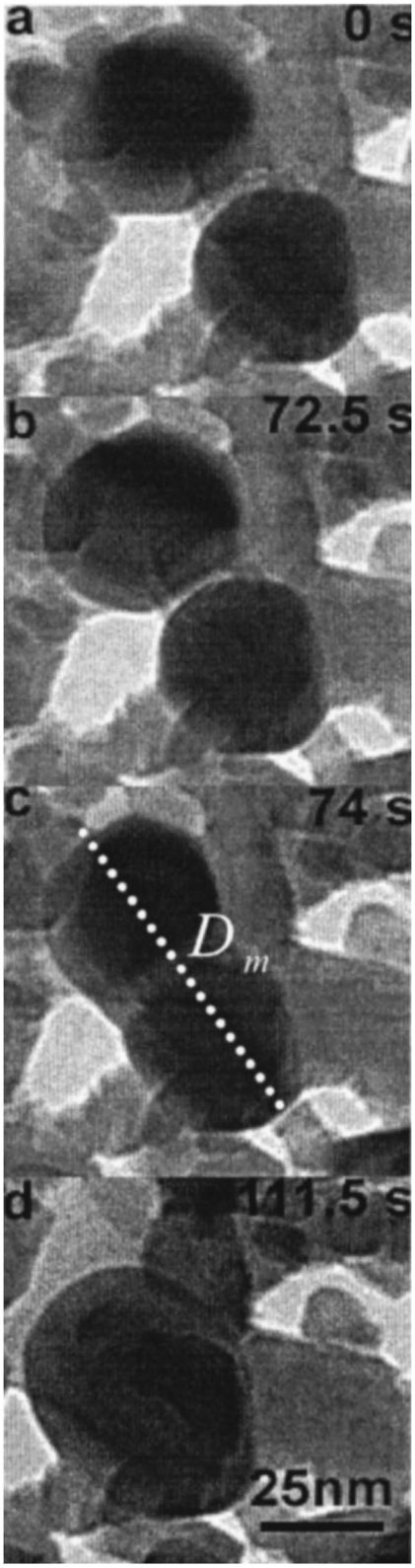

FIG. 2. Sequence of TEM pictures showing various stages of coalescence of two cobalt particles of similar size during heat treatments at 850 °C. [(a) and (b)] Particle movements prior to coalescence. [(c) and (d)] stages of nanoparticle coalescence. The dotted line indicates the maximum distance between the particles.

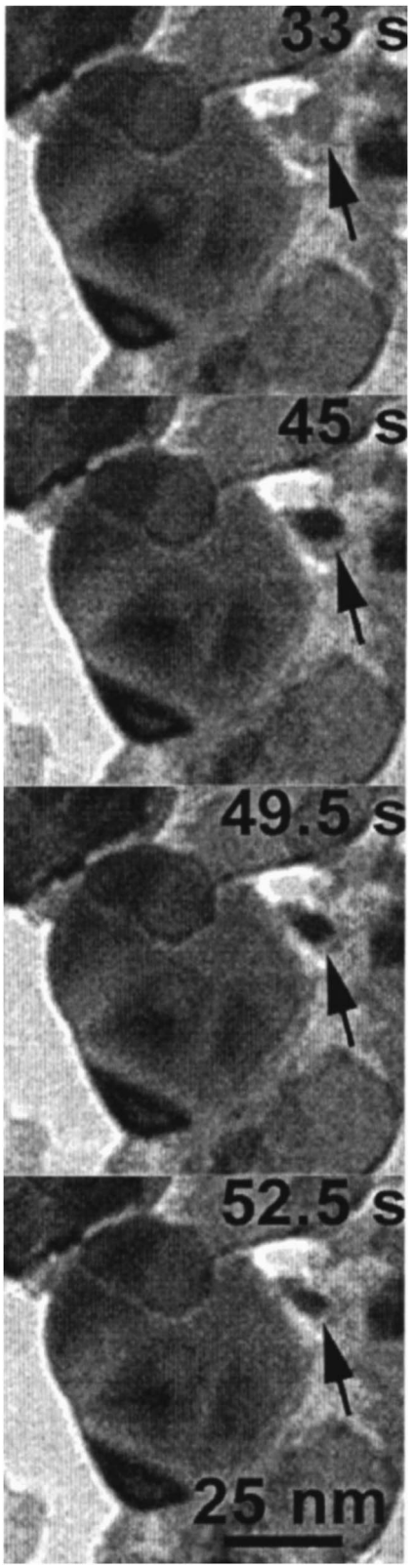

FIG. 3. Successive stages of small particle coalescence onto a large one during annealing at 700 °C. The arrow indicates the position of the small particle.

with the substrate remain rather immobile which is explained from the fact that their adhesion to the substrate is larger due to possible partial submersion. This can be explained by the fact that the surface energy of Co [γ=2.8 J/m^2 (Ref. 17) is larger than that of the substrate, i.e., γ_{Si}=1.4 J/m^2].[17]

Figure 2 also shows that the coalescence upon neck formation is accelerated in comparison with the slow initial stages where the particles move and adjust themselves to conform to each other in an arc-shaped curve of length com-

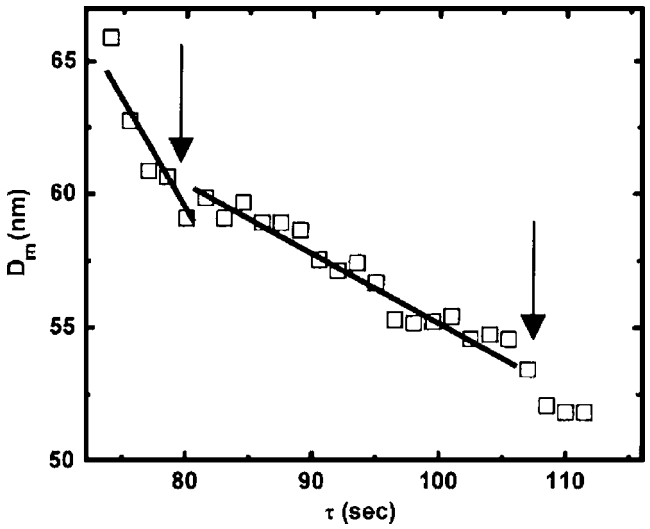

FIG. 4. Detailed time evolution of the maximum end-to-end distance (e.g., dotted line in Fig. 2) D_m after coalescence commences. The two regimes of linear behavior are indicated by the arrows. After the second arrow a saturation is observed since the particle has reached its final size.

parable with the particle radius R. For direct comparison, this behavior is also shown in Fig. 4 where the evolution of the maximum particle-particle distance D_m is plotted as a function of annealing time τ after coalescence begins ($\tau > 72$ s). For these particles necking occurs simultaneously over a significant contact area within $\sim 1-2$ s, which is fast in comparison with the previous (particle motion and position-shape rearrangement) and the follow-up of particle coalescence. This picture of particle coalescence does not support the theoretical suggestions[15,18] where the growth of necking occurs in short time starting from a point contact and followed by a rather slow increase at longer times. The short-time behavior was attributed to elastic and plastic particle deformations after come in contact, which were neglected in the analytical model given by Eq. (1).[16]

At long-time scales the presence of facets can substantially slow down surface diffusion while the model calculation in Eq. (1) (Ref. 16) assumes the particles to be perfectly spherical. On the other hand, in Fig. 2 the formation of facets is rather weak, and at these high annealing temperature we expect insignificant influence if any at all. Moreover, as the neck grows the surface area of the merging particles decreases, leading to the release of surface energy as heat that enhances atomic diffusion.[18] An estimation of the increase of particle temperature ΔT from the equation,[18]

$$\Delta T = \frac{3\sigma}{\rho c_\nu} \frac{1}{R_2} \frac{[1+(R_1/R_2)^2]-[1+(R_1/R_2)^3]^{2/3}}{[1+(R_1/R_2)^3]}, \tag{2}$$

where assuming $R_1 = R_2 = 15$ nm yields $\Delta T \sim 16$ K. Bulk values are assumed for surface tension σ, the heat capacity c_ν, and the bulk density ρ, which is justified considering the relatively large particle sizes of about 30 nm. The large size of R is the main reason why ΔT is small since $\Delta T \sim 1/R$. Thus, the latter mechanism is not expected to play any major role during coalescence. The evolution of the end-to-end distance D_m (as shown in Fig. 2) shows a linear decay at short-time scales $D_m = 142.4 - 1.05\tau$ which switches to a slower linear decay at longer-time scales $D_m = 80.3 - 0.25\tau$ as shown in Fig. 4. Thus, after necking occurs a transient period of relatively fast coalescence occurs followed by a slower coalescence rate at constant speed towards a single particle with partial spherical shape. In solids a nonspherical final shape can occur because the surface energy gradient (driving toward the spherical shape-minimum surface energy) cannot overcome the resistance imposed by the crystal structure (rearrangement of the lattice structure). Figure 4 actually shows the shrinkage due to transport processes that decrease the interparticle spacing as neck growth proceeds. The shrinkage, starting at $D_m^{(0)}$, is related to the neck size and can be formulated as[19,20]

$$\frac{D_m - D_m^{(0)}}{D_m^{(0)}} = -A \frac{t^{2/p}}{D_m^{2q/p}}, \tag{3}$$

where t is the isothermal sintering time, A depends exponentially on temperature, and the parameters p and q reflect the various stages of sintering, i.e., surface diffusion ($p=7$, $q=4$), grain-boundary diffusion ($p=6$, $q=4$), and bulk diffusion ($p=5$, $q=3$), respectively.[19,20] None of these mechanisms predict the correct slopes shown in Fig. 4. However, it should be pointed out that neck growth and formation of new contacts during sintering makes a quantitative description of the shrinkage of irregularly packed particles as in our case by relations derived for only two particles rather questionable. Actually, the agreement between experimental results and the shrinkage [Eq. (3)] for an agglomerate of clusters may be rather fortuitous. Further, in Eq. (3) any crystallographic influence has been neglected.

Recent theory investigations of the coalescence of Au nanoparticles larger than 2 nm at temperatures near the melting point[21] showed that after neck formation the dominant mechanism can be solid-state self-diffusion driven by stress gradients resulting from particle nonsphericity. It was also shown that the initial particle arrangement has an influence on the entire coalescence process.[21] When the particle is rotated it makes a smaller initial contact area between the two particles and thus a larger potential gradient yielding to faster evolution.[21] During neck formation, a small lattice rearrangement begins and the two particles have a small relative rotation. Similar behavior was observed in the previous works for Au (experimental) (Ref. 22) and Cu (numerical) (Ref. 23) nanoparticles. The rotation is even stronger when the initial lattice arrangement of the particles is very different (for temperatures below the melting temperature). In our case, however, we observed (first two stages in Fig. 2) the relative motion and possible particle reorientation to take place also prior to neck formation over a finite area. We should also point out that molecular-dynamics (MD) simulations indicated that the melting temperature of the coalescing system is well below that of the free single nanoparticle with the same particle size and can influence the coalescence process for nanoparticle sizes, i.e., below 3 nm.[24]

IV. CONCLUSIONS

In conclusion, we have examined coalescence phenomena of nanometer size Co nanoparticles by means of TEM. It

is found that Co nanoparticles in contact with the substrate are immobile; whereas those on top of other Co particles can move more easily during high-temperature annealing and coalesce. Indeed, during the coalescence of similar size particles, they rearrange themselves in an arc-shaped area leading to direct neck formation and thereafter to coalescence. Our observations do not support the theoretical predictions where a necking occurs at short times assuming an initial pathway of a point contact. However, they support theory predictions where particle rotation occurs at initiation of coalescence with a finite neck size leading to particle fusion and sphericization. Moreover, it was shown that after necking a transient period of relatively fast coalescence occurs followed by a slower coalescence rate at constant speed towards a single particle with partial spherical shape. The coalescence is faster with decreasing particle size, where in the case of unequal size the smallest particle is absorbed by an adjacent larger in an Ostwald ripening process.

Notably our observations show similarities and differences with theory predictions. This is not surprising since, for example, the particles exhibit facets, edges, polymorphism, and structural transitions that are not taken all into account in microscopic treatments.[15,18,21] The speed of coalescence has important consequences for the structure and morphology of nanoparticle-assembled materials.[25] Indeed, the formation of compact or ramified assemblies depends critically on the ratio between the coalescence time τ_c and the time τ_R it takes for a new particle to join an existing group. If $\tau_c/\tau_R > 1$ then ramified objects are formed, while in for $\tau_c/\tau_R < 1$ compact objects will be formed with the material having no memory of the initial building blocks.[15]

ACKNOWLEDGMENTS

We would like to acknowledge financial support from the Materials Science Centre MSC^{plus} program and the Netherlands Institute for Metals Research.

[1] O. S. Edwards and H. Lipson, Proc. R. Soc. London, Ser. A **180**, 268 (1943).
[2] A. R. Troiano and J. L. Tokich, Trans. Metall. Soc. AIME 195, 728 (1948).
[3] E. A. Owen and D. M. Jones, Proc. R. Soc. London, Ser. B 67, 456 (1954).
[4] R. E. Cech and D. Turnbull, J. Met. **8**, 124 (1956).
[5] W. C. Leslie and R. L. Miller, Trans. ASME 57, 972 (1964).
[6] Y. Fukano, Jpn. J. Appl. Phys. **13**, 1001 (1974).
[7] C. G. Granqvist and R. A. Buhrman, J. Appl. Phys. **47**, 2200 (1976).
[8] K. Kimoto and I. Nishida, J. Phys. Soc. Jpn. **22**, 744 (1967).
[9] S. Gangophdhyay, G. C. Hadjipanayis, S. M. Sorensen, and K. J. Klabunde, IEEE Trans. Magn. **28**, 3174 (1992); J. P. Chen, C. M. Sorensen, K. J. Klabunde, and G. C. Hadjipanayis, J. Appl. Phys. **76**, 6316 (1994); E. Anno, Phys. Rev. B **50**, 17 502 (1994); J. Jiao, S. Seraphin, X. Wang, and J. C. Withers, J. Appl. Phys. **80**, 103 (1996), and references therein.
[10] M. Hansen, *Constitution of Binary Alloys* (McGraw-Hill, New York, 1958).
[11] O. Kitakami, H. Sato, Y. Shimada, F. Sato, and M. Tanaka, Phys. Rev. B **56**, 13849 (1997).
[12] H. Sato, O. Kitakami, T. Sakurai, Y. Shimada, Y. Otani, and K. Fukamichi, J. Appl. Phys. **81**, 1858 (1997).
[13] H. Haberland, M. Moseler, Y. Qiang, O. Rattunde, T. Reiners, and Y. Thurner, Surf. Rev. Lett. **3**, 887 (1996).
[14] A. S. Edelstein and R. C. Cammarata, *Nanomaterials: Synthesis, Properties, and Applications* (Institute of Physics, Bristol, 1998).
[15] L. Lewis, P. Jensen, and J.-L. Barrat, Phys. Rev. B **56**, 2248 (1997).
[16] W. W. Mullins, J. Appl. Phys. **28**, 333 (1957); F. A. Nichols and W. W. Mullins, *ibid.* **36**, 1826 (1965).
[17] C. G. Zimmermann, M. Yeadon, K. Nordlund, J. M. Gibson, and R. S. Averback, Phys. Rev. Lett. **83**, 1163 (1999).
[18] S. Hendy, S. A. Brown, and M. Hyslop, Phys. Rev. B **68**, 241403 (2003).
[19] J. T. M. De Hosson and R. Popma, Diffus. Defect Data, Pt. A A218, 51 (2003).
[20] R. M. German, *Sintering Theory and Practice* (Wiley, New York, 1996).
[21] S. Arcidiacono, N. R. Bieri, D. Poulikakos, and C. P. Grigoropoulos, Int. J. Multiphase Flow **30**, 979 (2004).
[22] S. Iijima, P. M. Ajayan, and P. M. Substrate, J. Appl. Phys. **70**, 5138 (1991).
[23] H. L. Zhu and R. S. Averback, Mater. Manuf. Processes **11**, 905 (1996); Philos. Mag. Lett. **73**, 27 (1996).
[24] S. J. Zhao, S. Q. Wang, Z. Q. Yang, and H. Q. Ye, J. Phys.: Condens. Matter **13**, 8061 (2001).
[25] L. Bardotti, P. Jensen, A. Hoareau, M. Treilleux, and B. Cabaud, Phys. Rev. Lett. **74**, 4694 (1995); Surf. Sci. **367**, 276 (1996).